Available online at www.sciencedirect.com
ScienceDirect
Journal of Molecular Catalysis A: Chemical 258 (2006) 185–190
JOURNAL OF MOLECULAR CATALYSIS A: CHEMICAL
www.elsevier.com/locate/molcata

A novel photocatalyst $PbSb_2O_6$ for degradation of methylene blue

Ke-Lei Zhang [a,b], Xin-Ping Lin [a,b], Fu-Qiang Huang [a,*], Wen-Deng Wang [a,b]

[a] *Shanghai Institute of Ceramics, Chinese Academy of Sciences, Shanghai 200050, China*
[b] *Graduate School of the Chinese Academy of Sciences, Beijing 100039, China*

Received 17 January 2006; received in revised form 15 May 2006; accepted 19 May 2006
Available online 30 June 2006

Abstract

$PbSb_2O_6$ powder was synthesized by a solid-state reaction method. The specimen was characterized by X-ray diffraction and UV–vis diffuse reflectance spectra. $PbSb_2O_6$ has an intrinsic indirect band gap of 3.54 eV. Generally, the photocatalytic activity for degrading methylene blue over $PbSb_2O_6$ is higher than that over rutile-type TiO_2 under UV light illumination. The catalytic performance was discussed in close conjunction with the calculated band structure and crystal structure. The mechanisms of the pH-dependent photodegradation were proposed. The effects of photocatalyst concentration and Pt loading in suspending aqueous solution were also presented.

Keywords: Photocatalysis; $PbSb_2O_6$; Pt loading; TiO_2; MB

1. Introduction

Very recently, p-block metal oxides are gaining interest of researchers because of their capacities to photochemically split water. A series of such novel compounds as $ZnGa_2O_4$ [1], Zn_2GeO_4 [2], $AInO_2$ (A = Li, Na) [3], MIn_2O_4 (M = Ca, Sr, Ba) [4–6], Sr_2SnO_4 [6], $NaSbO_3$ [6,7], $M_2Sb_2O_7$ (M = Ca, Sr) [7], $CaSb_2O_6$ [7], $CaBi_2O_4$ [8] and $ZnBi_{12}O_{20}$ [9] have been reported. It is commonly accepted that photocatalytic activity is in close conjunction with structural features. Many efforts have been made to try to establish a correlation between local structures and photocatalytic activities [10–12]. It is generally revealed that local electric fields caused by the dipole moments in distorted metal–oxygen polyhedra favor efficient photoexcitation, delocalization and migration of charges. For example, the presence of the dipole moments in heavily distorted TiO_6 octahedra for $A_2Ti_6O_{13}$ (A = Na, K, Rb) and $BaTi_4O_9$ with tunnel structures contributes to high catalytic performance [13–15]. The RuO_2 or Pt dispersion on the powder surface achieved by a wet chemistry method causes a sharp increase in photocatalytic activity for H_2 production from water because of a uniform distribution of the fine particles on a 'nest' formed by the specific tunnel structure [16,17].

For another type of interesting photocatalysts with layered structures such as $A_2Ti_nO_{2n+1}$ (n = 2–4, A means alkali metal) [18] and $A_4Nb_6O_7$ [19], besides contributions of distorted local structures, the formation of static electric fields between negatively charged layer sheets constructed with corner- and/or edge-shared TiO_6 (NbO_6) octahedra and A^+ in the interlayer also prompts the delocalization of photoinduced charge carriers. Moreover, the photocatalytic activity can be substantially enhanced by modifying the layered structures by the construction of pillars of a semiconductor and/or a noble metal through an ion exchange reaction method [20].

In a study concerning the comparison of $Sr_2Ta_2O_7$ and $Sr_2Nb_2O_7$ layered perovskite photocatalysts [21], the structural parameter of the bond angle of M–O–M (M = Ta, Nb) was found to be closely related to photocatalytic performance, which reveals that the closer the bond angle is to the ideal 180°, the more easily electron–hole pairs can be delocalized. Similar results were obtained in the comparison between $InNbO_4$ and $InTaO_4$ [22].

The common principles on structure–property relationship stated above are concluded based on d-block oxide photocatalysts. For the p-block photocatalysts, they are also proved to be available [1–7]. Additionally, high photocatalytic activity may be partially ascribed to the high mobility of the photogenerated carrier in the hybridized energy bands [8,9].

In the present paper, we report another novel p-block metal oxide, $PbSb_2O_6$, for the photocatalytic degradation of methylene

* Corresponding author. Tel.: +86 21 52411620; fax: +86 21 52413903.
E-mail address: huangfq@mail.sic.ac.cn (F.-Q. Huang).

1381-1169/$ – see front matter © 2006 Elsevier B.V. All rights reserved.
doi:10.1016/j.molcata.2006.05.044

blue. Effects of powder concentration in suspending aqueous solution, pH value and Pt loading on photocatalytic properties were investigated. The photocatalytic activity was discussed in connection with band structure and crystal structure. The mechanisms of pH-dependent photodegradation were proposed.

2. Experimental

$PbSb_2O_6$ powder was synthesized by a solid-state reaction method. PbO and Sb_2O_3 with the purity of 99.99% were used as raw materials. Both the reagents were purchased from Sinopharm Chemical Reagent Co. (Shanghai, China) and used without further purification. Mixed powders with the stoichiometric proportion were calcined at 873 K for 48 h in an alumina crucible in air. After grinding, powders were allowed to react at 1023 K for 12 h. The formation of the metal oxides was confirmed by X-ray diffraction pattern. The band gap was estimated by UV–vis diffuse reflectance spectrum. Band calculation was conducted utilizing a self-consistent, scalar relativistic linearized muffin-tin orbital program (TB-LMTO) [23–25]. In order to increase the photocatalytic efficiency, platinum metal was loaded on the surface of $PbSb_2O_6$ by a wet chemical reduction method [16] under UV irradiation for 10 h, utilizing H_2PtCl_6 as a Pt source, followed by 10 h drying at 393 K in air.

The catalytic reaction for the degradation of 10 mg/L MB aqueous solution was carried out in a quartz cell with a cycled water system. The volume of initial MB solution is 300 mL. A 300 W high-pressure mercury lamp with a maximum emission at 365 nm was used for irradiation. The powder concentration in the MB aqueous solution ranges from 0.1 to 0.4 g/100 mL. Diluted NH_3 aqueous was used to adjust pH value of the suspending solution. UV illumination was conducted after the suspension was magnetically stirred in the dark for 50 min to reach adsorption–desorption equilibrium. During irradiation, about 5 mL suspension was continually taken from the reaction cell at given time intervals. The MB concentration in suspension was measured on a Hitachi UV-3010 spectrophotometer after centrifuging.

3. Results and discussion

3.1. Characterization of as-prepared powder

The mean particle size of the synthesized powder is about 3.8 μm. Its phase is confirmed by XRD pattern as shown in Figs. 1 and 2 is the UV–vis diffuse reflectance spectrum. The absorption edge is approximately 350 nm, corresponding to the intrinsic band gap of 3.54 eV. The conduction band (CB) edge position at the point of zero charge is estimated at 0.14 eV by utilizing the empirical formula expressed by $E_{CB} = X - E^e - 0.5E_g$ [26,27] where E_{CB} means the CB edge potential, X is the geometric mean of the Mulliken's electronegativities of constituent atoms, E^e is the energy of free electrons on the hydrogen scale (≈4.5 eV) and E_g is the band gap. Correspondingly, the valence band (VB) potential is calculated at about 3.68 eV. The value is more active than oxidative potentials of H_2O_2 and O_3, which are 1.77 and 2.07 eV, respectively.

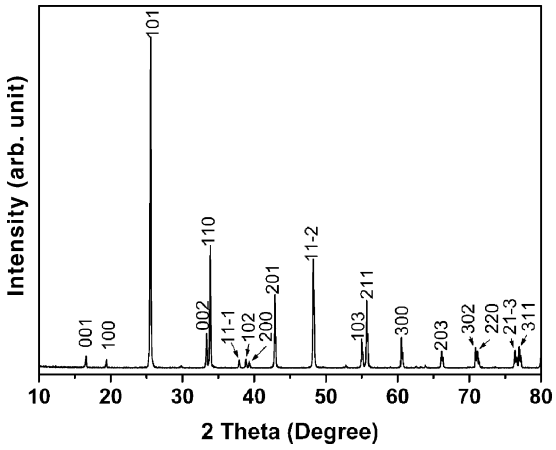

Fig. 1. XRD pattern of $PbSb_2O_6$.

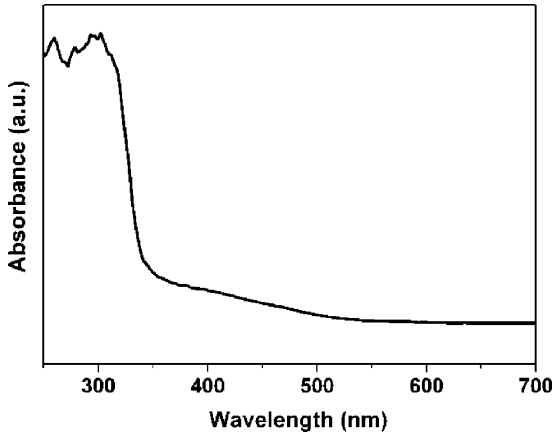

Fig. 2. UV–vis diffuse reflectance spectrum of $PbSb_2O_6$.

Thus, $PbSb_2O_6$ is believed to possess a much stronger ability of oxidation.

3.2. Band structure

Fig. 3 shows the calculated band structure of $PbSb_2O_6$. The valence band maximum (VBM) lies around in the middle of

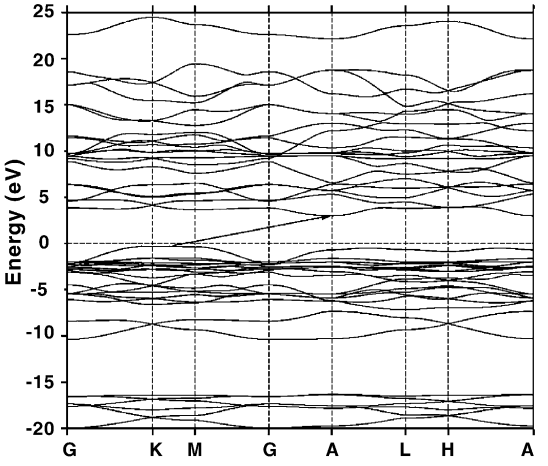

Fig. 3. Calculated band structure of $PbSb_2O_6$.

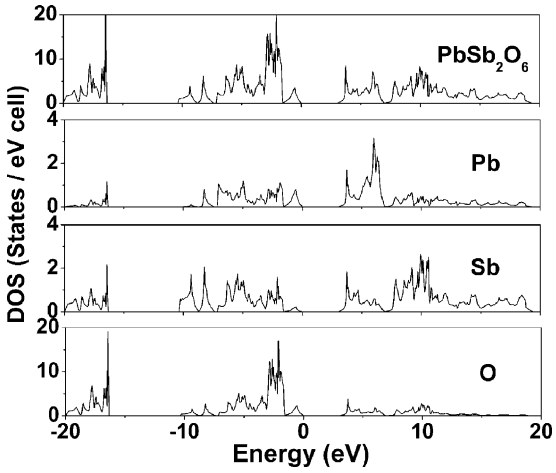

Fig. 4. Calculated total density of states and partial density of states.

KM line while the conduction band minimum (CBM) is located at A point. This means that $PbSb_2O_6$ is an indirect-gap material. A minimum forbidden gap between VBM and CBM is ca. 2.96 eV, which is lower than the experimental result of 3.54 eV. The reason for the difference may be that the discontinuity in the exchange-correlation potential is not taken into account in theoretical calculation, underestimating the energy gap between unoccupied and occupied orbitals.

Fig. 4 presents the calculated total density of states (TDOS) and partial density of states (PDOS). The valence band in the range of −5.0 to 0 eV is mainly composed of O 2p orbitals, hybridized by Sb 4d and Pb 6s orbitals to some extent. The hybrid conduction band at about 3.0–7.5 eV primarily consists of Sb 5s and Pb 6p orbitals. The hybrid states in valence and conduction bands may imply a fair mobility of photogenerated charges, favoring photocatalysis. The calculated results also show that Sb^{5+} and Pb^{2+} ions are active sites for photocatalysis, and hence, the structural features of both SbO_6 and PbO_6 polyhedra may have an important influence on photocatalytic performance which will be discussed in the following section.

3.3. Photocatalytic activity

3.3.1. Effect of powder concentration in suspension

Fig. 5 shows the influence of powder concentration in suspension on MB decomposition. In general, the percentage of decomposition higher than 95% over the photocatalyst with four different concentrations can be achieved as the irradiation time comes to 40 min. It can be also seen from the figure that the increasing powder concentration from 0.1 to 0.4 g/100 mL in the solution leads to enhanced degradation efficiency, but the rise in decomposition degree is small for the concentration rising from 0.3 to 0.4 g/100 mL owing to the stronger light reflection on the photocatalyst powder. In the present experiment, rutile TiO_2 with the average particle size of 1.5 μm was adopted as a control for the photocatalytic degradation of MB. As shown in Fig. 6, after 20 min UV irradiation, the MB removal on $PbSb_2O_6$ arrives at 76.2% for the powder concentration of 0.2 g/100 mL,

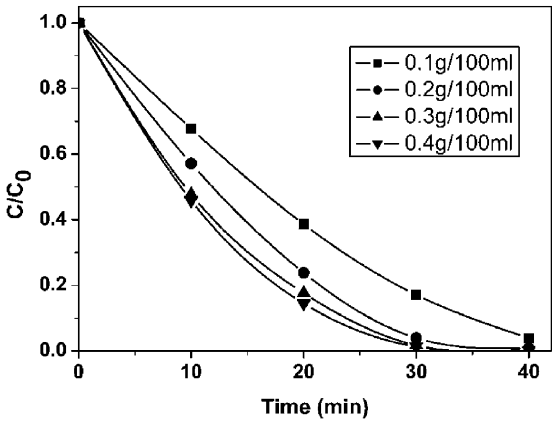

Fig. 5. Dependence of MB degradation on photocatalyst concentration in neutral (pH 6.86) suspension.

higher than 52.3% for rutile TiO_2 photocatalyst under the same experimental conditions.

3.3.2. Effect of Pt loading

In order to enhance the catalytic performance, Pt metal was loaded on the $PbSb_2O_6$ surface. The photocatalytic properties with different mass Pt dispersions are exhibited in Fig. 6. The presence of Pt leads to an increase in catalytic activity. Among the given loaded contents, the catalytic activity follows the decreasing order of 1% > 0.5% > 0%. The irradiation time for the complete MB decomposition is as short as about 20 min for 1 wt.% Pt addition, while 40 min for the pure $PbSb_2O_6$ powder. The MB decolorization rate in the reactor measured during initial 10 min UV light irradiation is ca. 0.216 mg/min for 1% Pt loaded powder and 0.113 mg/min for the pure phase powder. That is, 1% Pt dispersion roughly doubles the initial rate of MB removal. Since Pt is characteristic of a high electron conduction ability, the photoinduced electrons in the conduction band of $PbSb_2O_6$ are believed to readily transfer to that of Pt dispersed on $PbSb_2O_6$ surface, which facilitates photostimulated electron–hole separation and effectively inhibits their recombination.

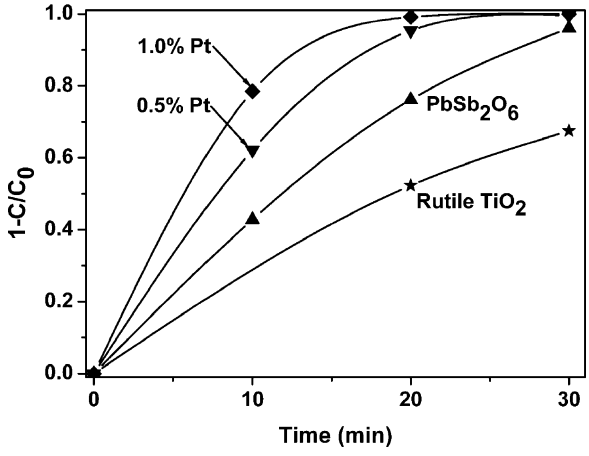

Fig. 6. Effect of Pt loading on MB photodegradation in neutral (pH 6.86) suspension.

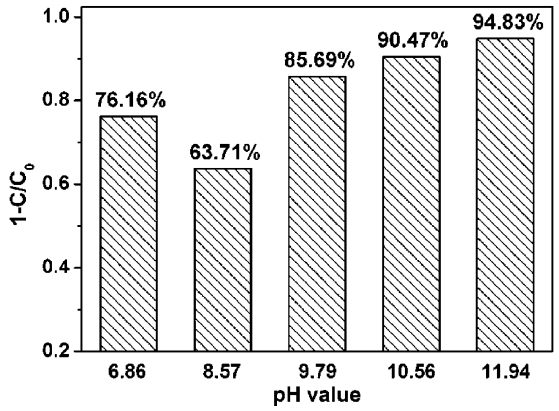

Fig. 7. Dependence of photocatalytic efficiency on pH value in suspending solution.

3.3.3. Effect of pH value

Fig. 7 presents the effect of pH value in the suspension on photocatalytic efficiency after 20 min irradiation. The variation of pH value shows its strong influence on the MB photodegradation. The photodegradation efficacies as a function of pH value decrease in the order of 11.9 > 10.6 > 9.8 > 6.9 > 8.6, where the conversion of MB at pH 11.9 and 6.8 are about 48.9 and 19.5%, respectively, higher than that at pH 8.6. It is generally accepted that the pH-dependent photodecomposition is mainly ascribed to the variations of surface charge properties of a photocatalyst. Consequently, this changes the adsorption behavior of a dye on catalyst surface. Since MB has a cationic configuration, its adsorption is favored in alkaline solution as demonstrated in Fig. 8. The increasing pH value results in a higher adsorption amount of MB on the $PbSb_2O_6$ surface. There is a sharp adsorption as pH ranges approximately from 8.5 to 10.5. This pH region may correspond to the point of zero charge for $PbSb_2O_6$. As MB decolorization takes place mainly on powder surface under the UV light irradiation, a suitable amount of MB in close contact with the catalyst may be effectively oxidized by positive holes or hydroxyl radicals. As seen comparatively in Figs. 7 and 8, the pH-dependent adsorption and photodecomposition are in good agreement when pH value is in the region from 8.6 to 11.9. At pH 6.9, however, the result seems to be controversial. The reason may be the formation of HO_2^- oxidant in the presence of H^+ by the following reaction equation,

$$H^+ + O_2 + 2e^- \rightarrow HO_2^- \quad (1)$$

which facilitates the MB oxidation under weakly acidic or neutral conditions [29].

There are three possible reaction mechanisms for the MB degradation in our experiments. For the UV light photocatalytic degradation over a catalyst, the initiation of this process could be described by from Eqs. (2) to (4), as well as the above Eq. (1), in which the generated $^\bullet O_2^-$, $^\bullet OH$ and HO_2^- could effectively oxidize the pollutant.

$$\text{catalyst} \rightarrow h^+ + e^- \quad (2)$$

$$e^- + O_2 \rightarrow {}^\bullet O_2^- \quad (3)$$

$$h^+ + OH^- \rightarrow {}^\bullet OH \quad (4)$$

For a photosensitization process with dye as a sensitizer, the initiation of this process could be depicted from Eqs. (5) to (8), in which the dye adsorbed on a catalyst was stimulated by UV light illumination and then a photoinduced electron on the dye transfers to the conduction band of the catalyst, subsequently reacts with molecular oxygen to form the $^\bullet O_2^-$ oxidant [30].

$$\text{dye}_{(ads)} \rightarrow \text{dye}_{(ads)}{}^* \quad (5)$$

$$\text{dye}_{(ads)}{}^* + \text{catalyst} \rightarrow \text{catalyst(e)} + \text{dye}_{(ads)}{}^+ \quad (6)$$

$$\text{dye}_{(ads)}{}^* + \text{catalyst} \rightarrow \text{dye}_{(ads)} + h^+ + e^- \quad (7)$$

$$\text{catalyst(e)} + O_2 \rightarrow \text{catalyst} + {}^\bullet O_2^- \quad (8)$$

The third mechanism for dye decomposition results from the photolysis process. Photocatalytic degradation of a dye is closely related to the structure stability of the dye, the adsorbability of the dye on catalyst surface, as well as the absorbance of the dye under light irradiation [31]. In other words, factors that can reduce dye stability, increase its adsorbability and intensify its light absorbance would effectively promote the photodegradation efficiency. Especially, the photocatalytic process and photolysis process are mainly associated with dye's structure stability, commonly measured by the energy required for decomposing dye molecular structure, i.e., the λ_{max} of dye; the photosensitization processes is primarily related to dye's adsorbability and light absorbance.

In neutral conditions, MB adopted in our experiments shows its instability upon UV light irradiation. The MB degradation by the pure photolysis in the blank experiment is about 17% after 30 min of light illumination. In a suspension with catalyst powders, however, it is impossible that there also exists such a large amount of MB removed by the photolysis mechanism, owing to the strong effects of the light diffraction and adsorption on powder surfaces. Therefore, we believe that in neutral or weak acidic conditions, the dye degradation is probably mainly controlled by the first photocatalytic mechanism, coordinatively with certain

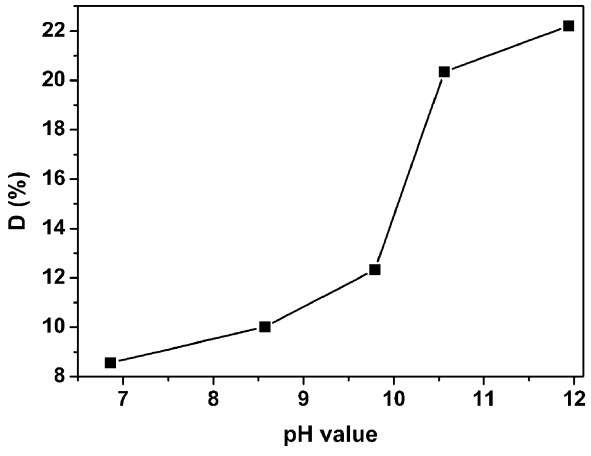

Fig. 8. pH-dependent adsorption of MB on powder surface, $D(\%) = (C_0 - C_e)/C_e \times 100$, where D is distribution ratio, C_0 means initial concentration of MB, C_e denotes equilibrium concentration [28].

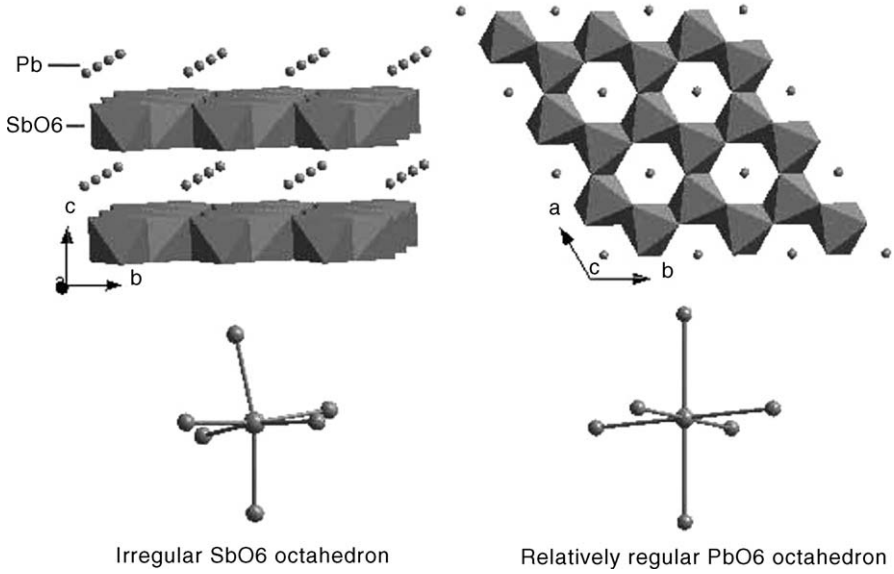

Fig. 9. Schematic representation of $PbSb_2O_6$ with layered configuration and M–O (M = Sb, Pb) polyhedra.

photosensitization and photolysis mechanisms. In alkaline conditions, the adsorbabilities of MB on the catalyst surfaces are increased. As a result, the dye removal rises from 63.7% at pH 8.6 to 94.8% at pH 11.9, as shown in Fig. 7. Such an obvious increase is mainly attributed to the photosensitization mechanism, because chemical reactions in the photocatalytic process cannot be intensified owing to the fact that λ_{max} of MB remains unchangeable in alkaline conditions. Hence, it is suggested that the initiation of decoloring MB in such an alkaline condition as pH 11.9, is most probably through the photosensitization mechanism, while the initiation of degrading MB in neutral or weak acidic conditions is probably dominated by the photocatalytic process.

3.4. Structure–property relationship

As stated above, $PbSb_2O_6$ is more active in MB photomineralization than rutile TiO_2. The reason is partially due to the oxidative potential of 3.68 eV, higher than the value of 2.94 eV for TiO_2 [32]. On the other hand, the special structure of $PbSb_2O_6$ crystal (shown in Fig. 9) will play an important role in the photocatalytic activity. $PbSb_2O_6$ has the hexagonal crystal structure, with the space group of *P*-31*m* (1 6 2) [33]. It exhibits a layered structure as viewed in the *a*- or *b*-axis, and a hexangular prism tunnel structure along the *c*-axis. One SbO_6 octahedron is connected by surrounding four octahedra by sharing edges, forming a layer sheet. The separated PbO_6 octahedra are located in interlayers, without any direct connections. The couplings between SbO_6 and PbO_6 octahedra are formed by sharing corners.

In the SbO_6, Sb–O bonds are similar in length, but the selected O–Sb–O angle varies much, from 79.543 to 96.209 Å. In comparison, PbO_6 is relatively regular in geometric configuration. In spite of the fair irregularity in local structures especially in SbO_6, it is calculated that the mass center of the O atoms in SbO_6 or PbO_6 is just sited at the metal position. That is, there exists no total dipole moment in the polyhedra, which causes no improvement in the photocatalytic performance. On the other hand, however, the presence of the layered configuration will induce static electric field between layers owing to different electronegativitis of Sb and Pb, facilitating photoexcited charge separation. In addition, the open configuration in tunnel structure $PbSb_2O_6$ is favorable for capillary adsorption of the reactants surrounding near the photocatalyst surface, enhancing catalytic properties.

It is believed that M–O–M angle has an important effect on charge migration. The closer the angle is to the ideal 180°, the less scattering and higher mobility occurs for photoinduced charges [21,22]. For $PbSb_2O_6$, the selected Sb–O–Sb and Sb–O–Pb angles are as high as 100.4° and 126.8°, respectively. This may also account for the catalytic activity of $PbSb_2O_6$.

4. Conclusions

$PbSb_2O_6$ powder was synthesized by the solid-state reaction method. It is an indirect-gap material with the intrinsic band gap of 3.54 eV. The valence band is mainly composed of O 2p orbitals, and the conduction band primarily consists of Sb 5s and Pb 6p orbitals. The results of MB degradation under UV light irradiation show that the photocatalytic activity of $PbSb_2O_6$ is higher than that of rutile-type TiO_2. The addition of 1 wt.% Pt doubles the catalytic efficiency during initial UV illumination. The specific layered and tunnel structures with irregular polyhedra, and the hybrid states in valence and conduction band as well as the deep oxidative potential are responsible for the high catalytic activity. The decolorization of MB in neutral or weakly acidic conditions is primarily through a photocatalytic process, while the MB photosensitization mechanism plays a more important role in alkaline conditions.

Acknowledgements

This research was financially supported by National Science Foundation of China Grant B010504-20471068. We thank Dr. Wei Tong and Dr. Weifeng Liu for their helpful discussions.

References

[1] K. Ikarashi, J. Sato, H. Kobayashi, N. Saito, H. Nishiyama, Y. Inoue, J. Phys. Chem. B 106 (2002) 9048.
[2] J. Sato, H. Kobayashi, K. Ikarashi, N. Saito, H. Nishiyama, Y. Inoue, J. Phys. Chem. B 108 (2004) 4369.
[3] J. Sato, H. Kobayashi, N. Saito, H. Nishiyama, Y. Inoue, J. Photochem. Photobiol. A 158 (2003) 139.
[4] J. Sato, N. Sato, H. Nishiyama, Y. Inoue, J. Phys. Chem. B 107 (2003) 7965.
[5] J. Tang, Z. Zou, M. Katagiri, T. Kako, J. Ye, Catal. Today 93–95 (2004) 885.
[6] J. Sato, N. Saito, H. Nishiyama, Y. Inoue, J. Phys. Chem. B 105 (2001) 6061.
[7] J. Sato, N. Saito, H. Nishiyama, Y. Inoue, J. Photochem. Photobiol. A 148 (2002) 85.
[8] J. Tang, Z. Zou, J. Ye, Angew. Chem. Int. Ed. 43 (2004) 4463.
[9] J. Tang, J. Ye, Chem. Phys. Lett. 410 (2005) 104.
[10] M. Kohno, S. Ogura, K. Sato, Y. Inoue, Chem. Phys. Lett. 267 (1997) 72.
[11] S. Ogura, M. Kohno, K. Sato, Y. Inoue, Phys. Chem. Chem. Phys. 1 (1999) 179.
[12] S. Ogura, M. Kohno, K. Sato, Y. Inoue, J. Chem. Soc., Faraday Trans. 93 (1997) 2433.
[13] W. Hofmeister, E. Tillmanns, W.H. Bauer, Acta Crystallogr. C 40 (1984) 1510.
[14] D.H. Templeton, C.H. Dauben, J. Chem. Phys. 32 (1960) 1515–1518.
[15] M. Kohno, S. Ogura, K. Sato, Y. Inoue, Chem. Phys. Lett. 319 (2000) 451.
[16] Y. Inoue, Y. Asai, K. Sato, J. Chem. Soc., Faraday Trans. 90 (1994) 797.
[17] W. Shangguan, A. Yoshida, Int. J. Hydrogen Energy 24 (1999) 425.
[18] S. Andesson, A.D. Wadsley, Acta Cryst. 15 (1962) 194.
[19] A. Kudo, A. Tanaka, K. Domen, K. Maruya, K. Aika, T. Onishi, J. Catal. 111 (1998) 67.
[20] M. Yanagisawa, S. Uchida, T. Sato, Int. J. Inorg. Mater. 2 (2000) 339.
[21] A. Kudo, H. Kato, S. Nakagawa, J. Phys. Chem. B 104 (2000) 571.
[22] Z. Zou, J. Ye, H. Arakawa, Chem. Phys. Lett. 332 (2000) 271.
[23] O.K. Andersen, Phys. Rev. B 12 (1975) 3060.
[24] O.K. Andersen, O. Jepsen, Phys. Rev. Lett. 53 (1984) 2571.
[25] O. Jepsen, O.K. Andersen, Z. Phys. B: Condens. Matter. 97 (1995) 35.
[26] A.H. Nethercot, Phys. Rev. Lett. 33 (1974) 1088.
[27] M.A. Butler, D.S. Ginley, J. Electrochem. Soc. 125 (1978) 228.
[28] Y. Shiraishi, N. Saito, T. Hirai, J. Am. Chem. Soc. 127 (2005) 12820.
[29] A. Gonzalez-Elipe, C.T. Munuera, J.J. Soria, J. Chem. Soc., Faraday Trans. 75 (1979) 749.
[30] C. Nasr, K. Vinodgopal, L. Fisher, S. Hotchandani, A.K. Chattopadhyay, P.V. Kamat, J. Phys. Chem. 100 (1996) 8436.
[31] W.S. Kuo, P.H. Ho, Dyes Pigments 71 (2006) 212.
[32] A. Fujishima, T.N. Rao, D.A. Tryk, J. Photochem. Photobiol. C 1 (2000) 1.
[33] R. Basso, G. Lucchetti, L. Zefiro, A. Palenzona, Eur. J. Mineral. 8 (1996) 487.